International Journal of Rock Mechanics & Mining Sciences 143 (2021) 104747

Contents lists available at ScienceDirect

International Journal of Rock Mechanics and Mining Sciences

journal homepage: www.elsevier.com/locate/ijrmms

Effect of the mineralogical composition on the elastoplastic hydromechanical response of Opalinus Clay shale

Eleonora Crisci [a,*], Alessio Ferrari [a,b], Silvio B. Giger [c], Lyesse Laloui [a]

[a] Ecole Polytechnique Fédérale de Lausanne (EPFL), Laboratory for Soil Mechanics (LMS), EPFL-ENAC-LMS, Station 18, CH-1015, Lausanne, Switzerland
[b] Università Degli Studi di Palermo, Department of Engineering, Viale Delle Scienze, Ed. 8, 90128, Palermo, Italy
[c] National Cooperative for the Disposal of Radioactive Waste, Nagra, Hardstr. 73, 5430, Wettingen, Switzerland

ARTICLE INFO

Keywords:
Opalinus clay
Shale
Mineralogy
Composition
Elasto-plasticity
Anisotropy

ABSTRACT

Opalinus Clay is the shale currently under investigation as the host formation for geological radioactive waste disposal in Switzerland. Its hydromechanical response has been widely studied, and the experimental results show a range of values whose dispersion needs to be clarified.

This work aims to explain the dispersion in the literature results by correlating the hydro-mechanical response to the mineralogical variability of the tested specimens.

Based on published microstructural studies, the Opalinus Clay shale is herein schematised as a sequence of two kinds of layers: the shaly (high in clay-mineral content) and the sandy (low in clay-mineral content) layers. The mineralogical composition, porosity and hydromechanical parameters are assigned to each layer type. The one-dimensional compressibility and the elastic response of combinations of layers are derived adopting an analytical solution for the stratified, transversely isotropic medium. The drained elastic properties are used to calibrate the approach, and the undrained elastic properties are derived and compared to literature data. Empirical correlations between the layer composition and the geomaterial strength are also drawn.

It is shown that by adopting a layered structure with an alternation of two kinds of layers, most of the variability in the studied geomechanical properties of Opalinus Clay can be captured.

1. Introduction

Opalinus Clay is a Jurassic age shale encountered in northern Switzerland and southern Germany, that for over two decades has been extensively studied as a possible host formation and natural barrier for engineering applications, such as radioactive waste disposal and CO_2 sequestration.

The shale has a very low porosity and permeability, good self-sealing potential and a relatively high mechanical strength. The combination of these characteristics makes Opalinus Clay an ideal geological barrier.[18] As common for sedimentary geomaterial (e.g., Ref. 3), it has a transversely isotropic behaviour; in the sedimentation direction, at the centimetre to decimetre scale, the formation presents a layered structure with alternating clay-rich and quartz-calcite rich layers, whose differences in composition have been attributed to the environmental conditions at the coastal basin during the deposition process.[7] At the scale of the Mont Terri Underground Rock Laboratory (URL) in the Jura Mountains (Switzerland), several lithostratigraphic subunits have been identified.[37] Because of their predominance in the sites of interest for practical applications, two of those facies are of primary importance: the shaly facies (a rather homogenous argillaceous shale with quartz-rich lenses) and the sandy facies (a more heterogeneous marly shale with lenses of sandstone).[38] In the past, much research focused on the behaviour of the more homogeneous shaly facies of the formation. In the last years, the evaluation of the feasibility of the engineering applications, led to a growing interest in the variability of the Opalinus Clay parameters, that need to be account to model the large-scale response of the underground; therefore an attempt to extend the current knowledge of Opalinus Clay towards the heterogenous sandy facies was conducted.

Prior studies highlighted that specimens of Opalinus Clay with higher quartz and carbonate contents showed a higher rigidity,[22] minor volumetric sensitivity to changes in total suction,[33] and lower compressibility and swelling indices in one-dimensional consolidation.[12] Attempts to relate the composition of the shale to the shear strength have been proposed in Ref. 25 using triaxial test results obtained on specimens with an unknown initial degree of saturation,[21,22] and showed dispersion in the results. The scatter in the results in Ref. 25

* Corresponding author.
E-mail address: eleonora.crisci@epfl.ch (E. Crisci).

https://doi.org/10.1016/j.ijrmms.2021.104747
Received 7 September 2020; Received in revised form 24 February 2021; Accepted 25 March 2021
Available online 23 May 2021

List of symbols

ϑ_i	Volumetric fraction of the *i* component
ϑ_{shaly}	Shaly volumetric fraction
ϑ_{sandy}	Sandy volumetric fraction
ρ_s	Solid density, g/m^3
$\rho_{s,c}$	Clay-minerals solid density, g/m^3
$\rho_{s,nc}$	Average solid density of material excluding the clay-minerals (nc = non-clay), g/m^3
σ'_{ij}	Effective stress tensor, Pa
σ_{ij}	Total stress tensor, Pa
ϕ'	Mohr-Coulomb parameter – friction angle, °
$\widetilde{\phi}_c$	Solid volume fraction of the clay component
$\widetilde{\phi}_{nc}$	Solid volume fraction of the non-clay component
$\widetilde{\phi}_{shaly}$	Volumetric solid fraction of the shaly layer, %
$\widetilde{\phi}_{sandy}$	Volumetric solid fraction of the sandy layer, %
ν_1^u, ν_2^u	Undrained Poisson's ratios
$\nu_{1,i\ (or\ j)}$	Poisson's ratio parallel to the bedding planes for the *i (or j)* layer
$\nu_{2,i\ (or\ j)}$	Poisson's ratio perpendicular to the bedding planes for the *i (or j)* layer
a	Clay volumetric fraction in the shaly layers
b	Clay volumetric fraction in the sandy layers
B	Skempton *B* pore water pressure coefficient
c'	Mohr-Coulomb parameter - cohesion, Pa
C	Volumetric compressibility of the transversely isotropic geomaterial, Pa^{-1}
C_c	Compressibility index
$C_{c,i}$	Compressibility index for the *i* component
e	Void ratio
e_0	Initial void ratio
$e_{1,i}$	Void ratio of the *i* component at a vertical load of 1 MPa
e_{shaly}	Void ratio of the shaly layer
e_{sandy}	Void ratio of the sandy layer
E_1, E_2	Young's modulus parallel and perpendicular to the bedding planes, Pa
E_1^u,E_2^u	Undrained Young's moduli, Pa
$E_{1,ref}$, $E_{2,ref}$	Drained Young's moduli reference value at 1 MPa, Pa
G_1	Shear modulus parallel to bedding, Pa
G_2	Shear modulus perpendicular to bedding, Pa
M_w	Mass of water, g
M_s	Solid mass, g
$M_{s,c}$	Solid clay mass, g
$M_{s,nc}$	Solid non-clay mass, g
$M_{s,c,shaly}$	Solid clay mass in the shaly layer, g
$M_{s,nc,shaly}$	Solid non-clay mass in the shaly layer, g
$M_{s,c,sandy}$	Solid clay mass in the sandy layer, g
$M_{s,nc,sandy}$	Solid non-clay mass in the sandy layer, g
p	Isotropic total stress, Pa
p'	Isotropic effective stress, Pa
q	Deviatoric stress, Pa
V_s	Volume of the solid material, m^3
V_v	Volume of voids, m^3
$V_{s,c}$	Volume of the solid clay fraction, m^3
$V_{s,nc}$	Volume of the solid non-clay fraction, m^3
$V_{s,c,shaly}$	Volume of the solid clay fraction in the shaly layer, m^3
$V_{s,nc,shaly}$	Volume of the solid non-clay fraction in the shaly layer, m^3
$V_{s,c,sandy}$	Volume of the solid clay fraction in the sandy layer, m^3
$V_{s,nc,sandy}$	Volume of the solid non-clay fraction in the sandy layer, m^3
$V_{v,shaly}$	Volume of voids in the shaly layer, m^3
$V_{v,sandy}$	Volume of voids in the sandy layer, m^3
x_c	Clay mass fraction
x_{nc}	Non-clay mass fraction

is to attribute both to the composition variability and the inconsistency in the degree of saturation of the specimens, which has been demonstrated to play a significant role in the mechanical response of shales and gas shales: the lower the degree of saturation is, the higher the strength and the stiffness will be.[9,16,17,32–34,39,46]

Recently, new sets of triaxial and oedometric tests were made available on saturated specimens of Opalinus Clay in the drained and undrained conditions.[11,12,14,15,20,35,36] In the triaxial tests, attention was paid to the saturation of the specimen (applying fluid backpressure higher than 2 MPa) and its verification performing Skempton's B tests. The strain rates to apply during shearing were calculated, considering the consolidation coefficient, to ensure homogenous pore pressure distribution within the specimen.[36]

The newly gathered experimental information in saturated conditions represents an opportunity to revise the response of Opalinus Clay, isolating the effect of the material composition on the mechanical behaviour from that of the degree of saturation.

Several studies considered the composition or layering structure to reproduce the behaviour of soil and rock. Early works proposed analytical solution to obtain elastic properties of transversely isotropic layered materials from the properties of the layers.[1,2,10,19,43] Later works showed experimentally (e.g. Refs. 2,24 or through numerical modelling (e.g., Refs. [49], 27) the effect of the alternation of soft and hard layers on the geomaterial strength and stiffness, with considerable computational costs. All the studies showed that the stiffness and strength of geomaterials decrease as the amount of clay content increases.

In this work, the variability in the mechanical properties of Opalinus Clay shale in the laboratory tests (centimetre scale) is shown to depend on the specimen composition and is interpreted adopting a layered structure model. Empirical correlations are derived and an analytical model, based on Ref. 43 is adopted to determine the elastic properties of the transversely isotropic geomaterial.

Based on published microstructural studies, the shale is herein schematised as an alternation of two kinds of layers (a clay-rich, softer layer, and a quartz-calcite rich, harder layer) with fixed mineralogical compositions and structures. The mechanical properties of the two kinds of layers are first calibrated with a subset of the available data. Then, the mechanical response for several proportions of the two-layer types is evaluated.

In this work, first, the adopted composition of the layers is discussed, and the derivation of a single material parameter (the shaly volumetric fraction) from the mineralogical composition is presented. Then, the non-linear elastic properties of the transversely isotropic material are presented, calibrated on a sub-set of the available data and then used to predict the elastic properties for a wide range of compositions. The layered structure is then adopted to interpret the one-dimensional compressibility and is used to construct empirical correlations with the shear strength of the Opalinus Clay.

2. Composition of the sandy and shaly layers

In several studies, the macro- and microstructure of samples collected in the Mont Terri Underground Rock Laboratory were analysed and the alternation of the sedimentary structures reported.[23,29,38,40,44] Observation of the core samples, including X-ray images, confirms the systematics structure of the Opalinus Clay,[26] in which an alternation of layers with higher clay content and layers with a higher quartz-calcite content is found, with a thickness of the layers of a few millimetres up

to several centimetres.

Correlations between the mineralogical composition and the specimen porosity have also been reported in several works.[12,23,31,40]

In this work, the characterization of the layer types presented in Ref. 23 is adopted. It is assumed that the Opalinus Clay can be schematised as a stratified material (Fig. 1) composed of parallel strata of variable thicknesses, in which two types of layers are distinguishable.[23] The clay-rich layers, hereafter called "shaly layers" (Fig. 1b) are composed of a clay matrix, with particles preferentially oriented along the bedding direction, in which the grains of other minerals–typically quartz and calcite–are immersed. In contrast, quartz/calcite-rich layers, hereafter called "sandy layers" (Fig. 1c), are mainly made of quartz grains, and the inter-grain space is occupied by clay particles, shifting the fabric to a grain-supported type as the quartz content increases. The sandy layers are found to have a lower porosity compared to the shaly layers. The shaly layers in specimens coming from the sandy and the shaly lithofacies of the formation were found to have a similar structure and clay-mineral composition, namely, in order of decreasing abundance, illite, kaolinite, illite-smectite mixed layers, and chlorite.[7] The specimens from the shaly facies are here assumed to be only composed of the shaly-type of layers, while in the specimens from the sandy facies of the formation an alternation of shaly and sandy layers of variable thicknesses is considered (Fig. 1d).

The volume of the shaly layers and sandy layers, divided by the total volume is defined as the sandy and shaly volumetric fractions ϑ_{sandy}, ϑ_{shaly}, respectively. The sum of the two fractions is equal to one.

The volumetric fractions are derived from the mineral fraction of the tested specimens adopting a fixed composition for the shaly and sandy layers. In particular:

- shaly layer: clay content $a = 65\%$ in volume, void ratio $e_{shaly} = 0.23$;
- sandy layer: clay content $b = 15\%$ in volume, void ratio $e_{sandy} = 0.11$.

The system of equations to derive the shaly and sandy volumetric fractions from the mineralogical composition is presented in the Appendix.

In Fig. 2, the correspondence between clay-mineral content x_c and shaly volumetric fraction ϑ_{shaly} for the whole range of clay-mineral contents is reported. The extremes of the curve correspond to the case in which only shaly layers or sandy layers compose the specimen.

The shaly volumetric fraction is used as the only input information for the geomaterial structure in the analysis of the mechanical properties of the layered geomaterial, presented in the following sections.

3. Elastic response

3.1. Nonlinear transversely isotropic elastic parameters in the drained and undrained conditions

Five independent parameters are needed to describe the elastic response of a transversely isotropic geomaterial. In addition, the elastic moduli of Opalinus Clay are known to be stress-dependent (e.g., Refs. 14,42).

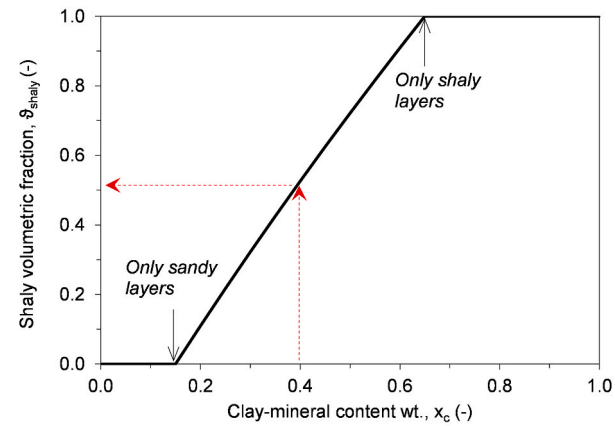

Fig. 2. Correlation between the clay-mineral content and the shaly fraction of the layered structure. The dotted arrows suggest the reading direction of the graph.

The adopted definition of the elastic parameters for a transversely isotropic material is explained in Fig. 3. The coordinate system in Fig. 3 is defined considering the bedding direction: directions 1 and 2 are in the plane of isotropy and direction 3 is perpendicular to it. In Fig. 3 and Equations (1)–(4), the relationships are written in incremental form, while the stress dependency is addressed later in this section.

In transversely isotropic conditions, the elastic laws are written as Equation (1).

$$\begin{pmatrix} \delta\varepsilon_{11} \\ \delta\varepsilon_{22} \\ \delta\varepsilon_{33} \\ \delta\varepsilon_{12} \\ \delta\varepsilon_{23} \\ \delta\varepsilon_{13} \end{pmatrix} = \begin{pmatrix} \frac{1}{E_1} & -\frac{\nu_1}{E_1} & -\frac{\nu_2}{E_2} & 0 & 0 & 0 \\ -\frac{\nu_1}{E_1} & \frac{1}{E_1} & -\frac{\nu_2}{E_2} & 0 & 0 & 0 \\ -\frac{\nu_2}{E_2} & -\frac{\nu_2}{E_2} & \frac{1}{E_2} & 0 & 0 & 0 \\ 0 & 0 & 0 & \frac{1}{2G_1} & 0 & 0 \\ 0 & 0 & 0 & 0 & \frac{1}{2G_2} & 0 \\ 0 & 0 & 0 & 0 & 0 & \frac{1}{2G_2} \end{pmatrix} \begin{pmatrix} \delta\sigma'_{11} \\ \delta\sigma'_{22} \\ \delta\sigma'_{33} \\ \delta\sigma'_{12} \\ \delta\sigma'_{23} \\ \delta\sigma'_{13} \end{pmatrix} \quad 1$$

The five parameters (E_1, E_2, ν_1, ν_2, G_2) are independent, while G_1 and ν_3 depend on the other parameters:

$$G_1 = \frac{E_1}{2(1+\nu_1)} \text{ and } \nu_3 = \nu_2 \frac{E_1}{E_2} \quad 2$$

Although it is an independent parameter, G_2 is often not measured because of the practical difficulties of obtaining it in the laboratory. Several authors have proposed correlations to estimate G_2 based on empirical observations, combining the other elastic parameters (e.g.

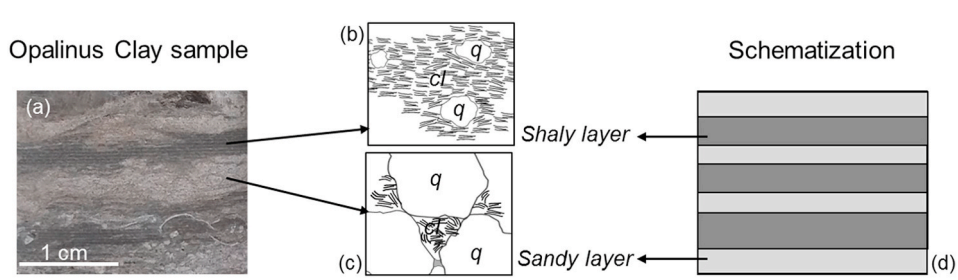

Fig. 1. Opalinus Clay as a layered material: (a) a sandy specimen picture; (b) shaly and (c) sandy layer structures (q: quartz, cl: clay matrix); and (d) schematic layered structure of a sandy specimen.

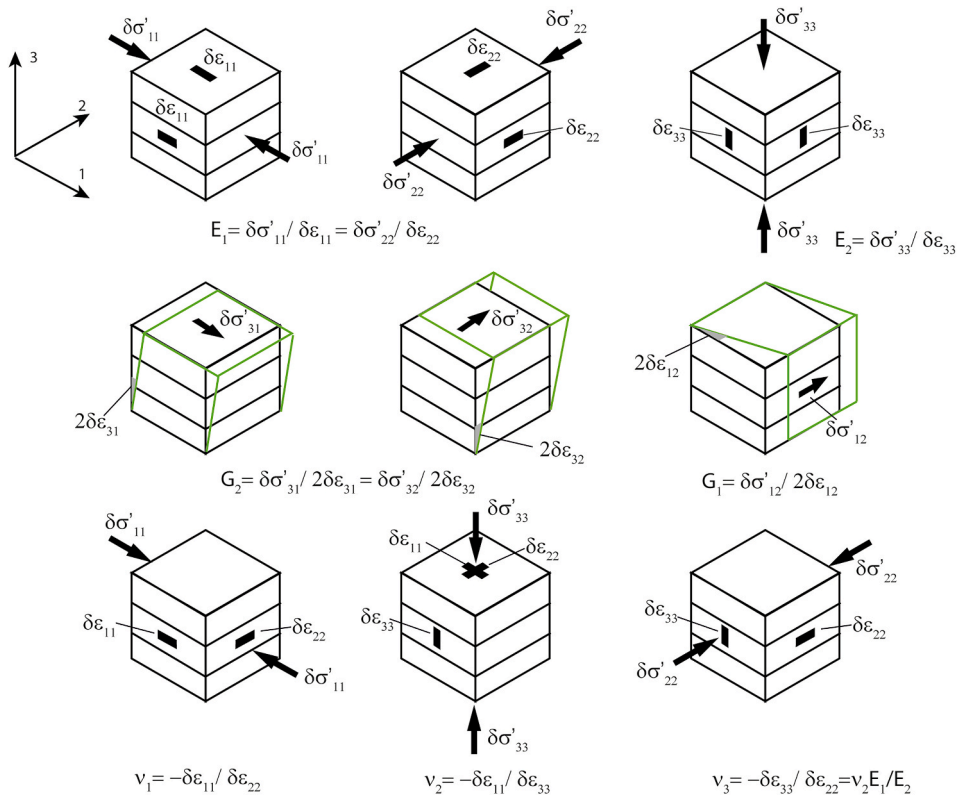

Fig. 3. Definition of the elastic parameters for a transversely isotropic material. Elements of the layered geomaterial are subjected to stresses in the principal directions (1,2,3). The elastic properties formulations are presented with reference to the various stress applied, and the corresponding strains.

Refs. 4,45,47) proposed the relationship $G_2=E_2/[2(1+\nu_2)]$, which is analogous to Equation (2) for G_1.

In experimental testing in triaxial conditions, cylindrical specimens are often cored with the cylinder axis either perpendicular (named S-specimen) or parallel (P-specimen) to the bedding orientation. In both cases, the directions 1, 2 and 3 in Fig. 3 are assumed to be aligned with the principal directions.

The transversely isotropic matrix further simplifies as follows:

$$\begin{pmatrix} \delta\varepsilon_{11} \\ \delta\varepsilon_{22} \\ \delta\varepsilon_{33} \end{pmatrix} = \begin{pmatrix} \frac{1}{E_1} & -\frac{\nu_1}{E_1} & -\frac{\nu_2}{E_2} \\ -\frac{\nu_1}{E_1} & \frac{1}{E_1} & -\frac{\nu_2}{E_2} \\ -\frac{\nu_2}{E_2} & -\frac{\nu_2}{E_2} & \frac{1}{E_2} \end{pmatrix} \begin{pmatrix} \delta\sigma'_{11} \\ \delta\sigma'_{22} \\ \delta\sigma'_{33} \end{pmatrix} \tag{3}$$

For specimens loaded perpendicular to the bedding, the two stress components in the radial direction, $\delta\sigma'_{11}$ and $\delta\sigma'_{22}$, are equal. For specimens loaded parallel to the bedding, the two equal stress components in the radial direction are $\delta\sigma'_{33}$ and $\delta\sigma'_{22}$ (directions in Fig. 3).

For the total stress, hereafter used for the undrained conditions, the matrix will be written as follows:

$$\begin{pmatrix} \delta\varepsilon_{11} \\ \delta\varepsilon_{22} \\ \delta\varepsilon_{33} \end{pmatrix} = \begin{pmatrix} \frac{1}{E_1^u} & -\frac{\nu_1^u}{E_1^u} & -\frac{\nu_2^u}{E_2^u} \\ -\frac{\nu_1^u}{E_1^u} & \frac{1}{E_1^u} & -\frac{\nu_2^u}{E_2^u} \\ -\frac{\nu_2^u}{E_2^u} & -\frac{\nu_2^u}{E_2^u} & \frac{1}{E_2^u} \end{pmatrix} \begin{pmatrix} \delta\sigma_{11} \\ \delta\sigma_{22} \\ \delta\sigma_{33} \end{pmatrix} \tag{4}$$

in which the elastic parameters with superscript u are obtained in the undrained conditions.

The equations relating the drained and undrained parameters have been independently derived by several authors (e.g., Refs. 6,30,41) assuming no drainage or cavitation and neglecting the volume compressibility of the solid grains.The authors in Ref. 6 also considered a value of Skempton's B coefficient (the increment of pore water pressure induced by an increment of mean total stress when isotropic stress is changed in undrained conditions) lower than 1, which is appropriate for shales:

$$\begin{aligned} E_2^u &= \frac{E_2 E_1^2 C}{E_1^2 C - B\left(\frac{E_1}{E_2} - 2\nu_2\right)^2 E_2} \\ E_1^u &= \frac{E_1^2 C}{E_1 C - B(1-\nu_2-\nu_1)^2} \\ \nu_2^u &= \frac{E_2}{E_1}\frac{\nu_2 E_1 C + B\left(\frac{E_1}{E_2} - 2\nu_2\right)(1-\nu_2-\nu_1)}{E_1 C - B(1-\nu_2-\nu_1)^2} \\ \nu_1^u &= \frac{\nu_1 E_1 C + B(1-\nu_2-\nu_1)^2}{E_1 C - B(1-\nu_2-\nu_1)^2} \\ C &= \frac{1}{E_1}\left(\frac{E_1}{E_2} - 4\nu_2 - 2\nu_1 - 2\right) \end{aligned} \tag{5}$$

with C the volumetric compressibility of the transversely isotropic geomaterial.

Opalinus Clay elastic parameters have been experimentally proved to depend on the stress state. Young's moduli E_1 and E_2 increase with the mean effective stress. On the other hand, for confining effective stress below 16 MPa, the Poisson's ratios seem to be only marginally affected by the stress state.[14,20] The Poisson's ratios are therefore assumed herein constant.

For the range of mean effective stress between 3 and 16 MPa, the evolutions of Young's moduli with the mean effective stress were interpolated with power laws:

$$E_1 = E_{1,ref}\left(\frac{p'}{p'_{ref}}\right)^{n_1} \text{ and } E_2 = E_{2,ref}\left(\frac{p'}{p'_{ref}}\right)^{n_2} \quad 6$$

where p' is the current mean effective stress, p'_{ref} is a reference value for the mean effective stress, $E_{1,ref}$ and $E_{2,ref}$ are the corresponding E_1 and E_2 values at the reference stress level, and n_1 and n_2 are two power-law parameters.

During unloading and reloading, shales present a hysteretic and nonlinear behaviour. For rocks, the hysteretic response is usually attributed to the presence of microcracks[3,13,48] that tend to slide after reaching the crack strength resistance. As a consequence, from an unloading-reloading cycle, several values of Young's moduli may be derived, depending on the selected strain and stress ranges. In Fig. 4, an example of the hysteretic and nonlinear response upon unloading is reported in the plane of the deviatoric stress (q) versus the deformation in the shearing direction (ε_a). The result refers to the drained shearing phase of a triaxial test on an Opalinus Clay specimen from the sandy facies (S-specimen)[11] used for the hydromechanical parameter evaluation. The confining effective stress for the reported example is $\sigma'_{11} = \sigma'_{22} = 4$ MPa.

Depending on the amplitude of the unloading-reloading loop, the secant moduli may vary significantly. In addition, at the inversion of the loading direction (load to unload and the opposite), friction between the piston and the frame of the loading system may be produced, reducing the actual load applied on the specimen, and altering the moduli computation in the first part of the curve. As a consequence, the first part of the unloading may result in a higher estimate of the stiffness.

In Fig. 4, several possible secant and tangent moduli at different unloading stages are shown, and it is highlighted that the possible Young's moduli vary over one order of magnitude, from 3.5 MPa to 35 MPa.

To cope with the abovementioned sources of uncertainty, in this work, the Young moduli for all analysed tests is computed as the tangent modulus during unloading for a fixed strain range, 0.02%–0.04% (Fig. 4), measuring the strain from the beginning of the unloading phase. The strain calculation refers to the initial specimen height. In the example of Fig. 4, for the mentioned strain interval, Young modulus $E_2 = 6$ MPa was calculated. The strain range was selected because it is common to all the analysed tests, and the potential artefacts originating from the first part of the curve are excluded.

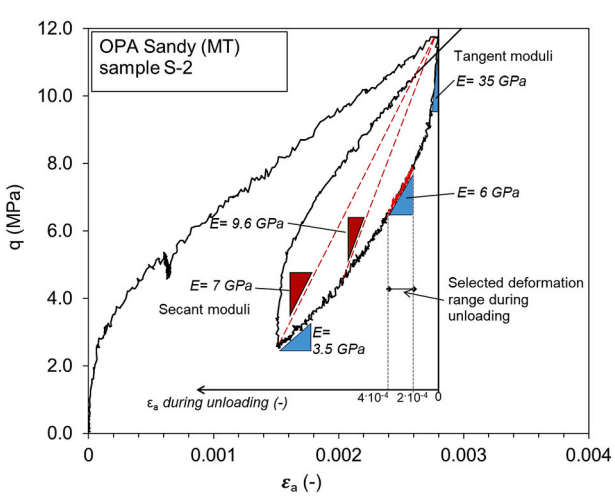

Fig. 4. Determination of the Young modulus during drained shearing of a sandy Opalinus Clay specimen. An unloading-reloading cycle during shearing is presented, showing the hysteretic response. Secant and tangent elastic moduli are shown to depend on the considered stress-strain interval. The deformation range 0.02%–0.04% from the begin of unloading is selected to compute Young modulus. The same interval is selected for each analysed test.

3.2. Elastic parameters dependency on the composition

As described in Section 2, the structure of the Opalinus Clay can be schematised as a layer alternation of shaly and sandy strata. In this section, the elastic properties of the stratified material at the specimen scale are inferred from the behaviour of the single stratum.

Given the stratification of the specimens, the elastic properties of a transversely isotropic continuum medium can be derived from the properties of the layers (Fig. 5), as analytically derived in several works.[2,10,19,43]

The equations for converting from the properties of the layers (Fig. 5a) to those of a continuum homogeneous medium (Fig. 5b) were derived based on the strain energy equivalence of the two media,[43] considering the following simplifying hypotheses: (i) each layer is homogeneous and transversely isotropic, (ii) the material remains continuous after deformation; (iii) the size of the specimen is at least the representative elementary volume and (iv) the variations in stresses and strains across the equivalent medium are negligible.

The micro and macrostructural studies presented in Section 2 support the applicability of the hypothesis (i): the composition of each layer type is consistent among specimens. No discontinuity between layers could be detected in elastic regime, in agreement with the hypothesis (ii). The size of the laboratory specimen (several centimetres) is more than 10 times larger than the coarser particles in the shale (in the silt-size order of magnitude) therefore considered sufficient to guarantee the representativeness of the specimen (iii). The assumption of negligible variation of stress and strain within the equivalent medium (iv) is assumed acceptable within a limited strain range, as the one adopted for the estimation of the elastic properties.

The resulting parameters (Equation (7)) are combinations of the parameters of each layer type and the corresponding volumetric fraction, ϑ_i, with i referring in this case either to the shaly or sandy fraction. Parameters without the i subscript refer to the equivalent continuum medium.

$$\begin{aligned}
\nu_1 &= \sum_i \frac{\vartheta_i \nu_{1i} E_{1i}}{1-\nu_{1i}^2} \Big/ \sum_i \frac{\vartheta_i E_{1i}}{1-\nu_{1i}^2} \\
\nu_2 &= (1-\nu_1)\sum_i \frac{\vartheta_i \nu_{2i}}{1-\nu_{1i}} \\
E_1 &= \left(1-\nu_1^2\right)\sum_i \frac{\vartheta_i E_{1i}}{1-\nu_{1i}^2} \\
E_2 &= \frac{1}{\sum_i \frac{\vartheta_i}{E_{1i}}\left(\frac{E_{1i}}{E_{2i}} - \frac{2\nu_{2i}^2}{1-\nu_{1i}}\right) + \frac{2\nu_2^2}{(1-\nu_1)E_1}} \\
G_2 &= \frac{1}{\sum_i \vartheta_i / G_{2i}}
\end{aligned} \quad 7$$

In the considered approach, the elastic properties can be derived by

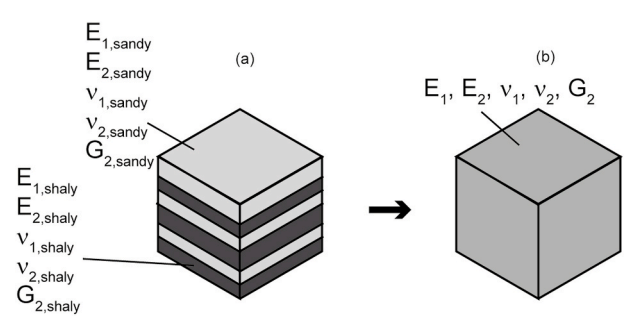

Fig. 5. (a) Stratified medium as an alternation of shaly and sandy layers and (b) a continuum homogeneous medium and the related elastic parameters.

neglecting the actual layer arrangement while considering the volumetric fraction of each layer kind.

3.3. Calibration of the drained elastic parameters of shaly and sandy layers

The elastic parameters for the shaly and sandy layers were obtained using the experimental results of saturated drained triaxial tests.[11,14] The layered structure proposed in Section 2 was adopted. The parameters for the shaly layers were calibrated on the elastic paths of tests on shaly specimens[14] that showed a transversely isotropic nonlinear behaviour.

Three tests on sandy specimens (shearing direction perpendicular to the layers, S-specimens)[11] were used to calibrate the sandy layer elastic parameter. The three tested specimens had shaly volumetric fractions of 20%, 20% and 30%.

Fig. 6 reports the elastic parameters obtained experimentally for shaly (E_1, E_2, ν_1 and ν_2) and sandy (E_2, ν_2) specimens as a function of the mean effective stress (the average value of p' in the selected strain range used for the computation of the elastic parameters). The data for E_1 and ν_1 are available only for the shaly specimens.[14] The nonlinear stress dependency of Young's moduli on the mean effective stress is highlighted. On the other hand, the variations in Poisson's ratio with the stress were found to be limited in the analysed confining stress range (<16 MPa) and neglected. A substantial difference was found between the Young's moduli of the shaly and sandy specimens: the E_2 of the sandy specimens are approximately twice those of the shaly specimens.

For each mean effective stress, the elastic parameters for the shaly and sandy layers can be derived from the specimen compositions.

As mentioned before, the shaly specimens are composed only of shaly layers. Therefore, the results for the shaly specimens directly provide the elastic properties of the shaly layer ($E_{1,shaly}$, $E_{2,shaly}$, $\nu_{1,shaly}$ and $\nu_{2,shaly}$).

The parameters of the sandy layer were back-calculated using Equation (7) and the information on the shaly layer and shaly volumetric fraction. Since only S-specimens are available for the sandy facies in the analysed stress range, E_1 and ν_1 are not derived. Therefore, the sandy layer is herein assumed to have an isotropic nonlinear response ($E_{1,sandy} = E_{2,sandy}$; $\nu_{1,sandy} = \nu_{2,sandy}$).

Equation (6) is applied for each layer to describe the evolution of Young's modulus with the mean effective stress. Poisson's ratios are assumed to be constant values. The obtained parameters are reported in Table 1.

The evolution of the elastic parameters of the specimens given by

Table 1
Parameters for the nonlinear evolution of Young's modulus and Poissson's ratios for each layer.

	E_{ref} (GPa)	n_1 or n_2 (−)	p'_{ref} (MPa)
$E_{1,shaly}$	1.8	0.48	1
$E_{2,shaly}$	1.8	0.35	1
$E_{1,sandy}$, $E_{2,sandy}$	2.4	0.57	1
$\nu_{1,shaly}$		0.10	
$\nu_{2,shaly}$		0.29	
$\nu_{2,sandy}$		0.20	

Equation (7) is depicted in Fig. 6 with the experimentally derived parameters. These calibrated trends match the dataset very well, showing that the selected forms for Equations (6) and (7) can describe the dependence of the elastic parameters on the stress level and the specimen composition.

3.4. Estimation of the undrained elastic properties

The drained elastic properties obtained from the calibration in Section 3.3 are here used to estimate the undrained elastic properties for the entire range of shaly volumetric fraction (Equations (5)–(7)). The evaluation was performed adopting equations in Ref. 6 for a B value equal to 0.8, compatibly with the values for Opalinus Clay in the considered confining effective stress range of 0–15 MPa.[14,20,35] The dependence of the B value on specimen composition is herein neglected, as no specific trend was identified within the mentioned stress range. The results are then compared with the experimental data from undrained triaxial tests.

Several undrained E_2^u values were obtained in Ref. 35 for S-specimens with a known mineralogical composition tested in saturated undrained conditions. The reported compositions were converted to shaly volumetric fractions. The drained elastic parameters were estimated using Equation (7) and then converted to undrained parameters using the correlations described in Section 3.1. If higher Skempton's coefficient are assumed, e.g., B = 1, the computed undrained elastic moduli are slightly higher than the results for B = 0.8, and the undrained elastic moduli are overestimated.

Fig. 7 shows Young's moduli in undrained conditions derived from the experimental testing and the computed estimate (lines) for various compositions with respect to the mean effective stress. The computed values provide a good match with the experimental results. The match is particularly accurate in the high shaly volumetric fraction range, while the procedure tends to slightly overestimate Young's modulus in the low

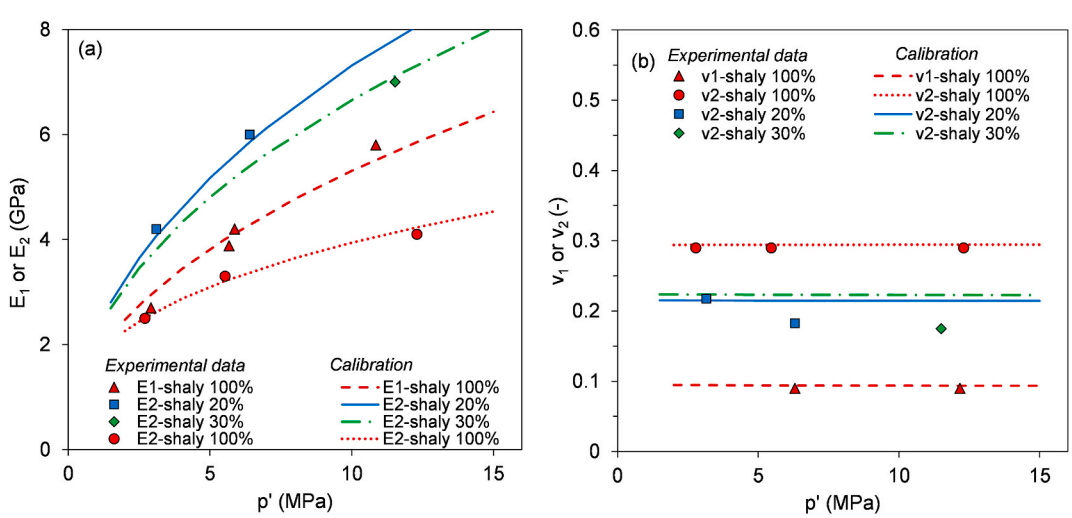

Fig. 6. Elastic moduli (a) and Poisson's ratio (b) versus the mean effective stress calibrated on the drained test results from 11 (shaly 20%, shaly 30%) and 14 (shaly 100%).

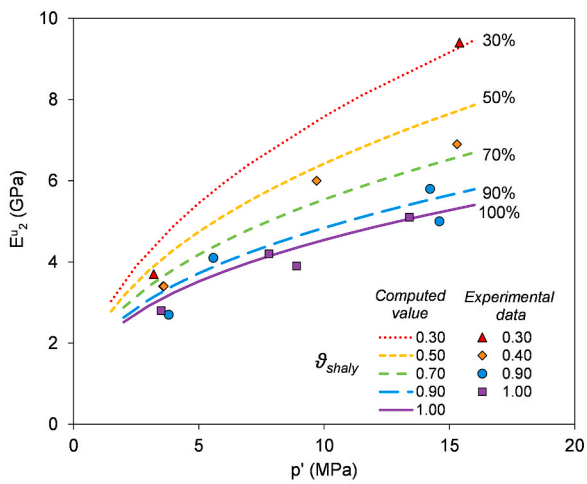

Fig. 7. Experimental data and computed value of E^u_2 for B = 0.8. Experimental data from Ref. 35.

shaly volumetric fraction range. Considering that the predictions are based exclusively on the clay content of each tested specimen, the correspondence is considered acceptable.

4. Elastoplastic compressibility

The Opalinus Clay response in oedometric conditions is determined based on the shaly volumetric fraction and two structural parameters, i.e. the reference void ratio for each layer type. Similar approaches were found to be widely used for clays in the literature.[5,8]

4.1. Compressibility of a layered geomaterial in oedometric conditions

Oedometric tests on Opalinus Clay have been presented in previous works[12,15] and allow for extrapolating information on the effect of the layering on the mechanical response. In Ref. 12, a positive correlation between the compressibility index and the clay-mineral content was drawn. The values of the compressibility index of S-specimens (i.e., loaded perpendicular to bedding direction) (Fig. 8) are herein reinterpreted adopting the definition of the shaly and sandy layers proposed in Section 2.

Considering the oedometric boundary conditions, the increment in the axial deformation of the layered specimen, $\delta\varepsilon_{33}$, can be computed as the sum of the change in the height of each layer divided by the total height of the specimen:

$$\delta\varepsilon_{33} = \frac{1}{h_t}\sum \frac{\delta\sigma'_{33}}{E_{oed,i}} h_i \qquad 8$$

where $\delta\sigma'_{33}$ is the increment of vertical stress, $E_{oed,i}$ is the oedometric

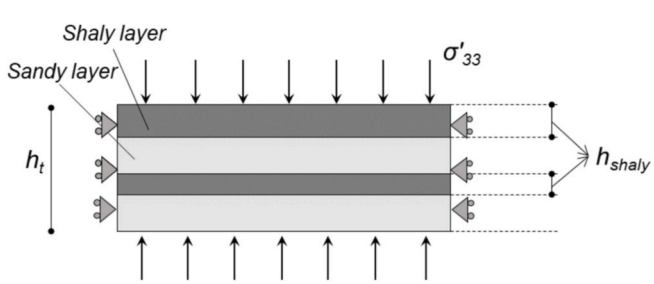

Fig. 8. Scheme of the stratified medium in oedometric conditions (lateral strain prevented). The thickness of the shaly layers (h_{shaly}) and total thickness (h_t) are presented.

modulus of the ith component for the loading step, h_i is the initial thickness of the layer i, and h_t is the initial total height. In the case of the two layer-type specimens, the thicknesses of the shaly and layers are summed, and the ratio $h_i/h_t = h_{shaly}/h_t$ corresponds to the volumetric fraction of the shaly layers (ϑ_{shaly}).

In the post-yield condition, Equation (8) can be written in terms of the compressibility index of each layer i ($C_{c,i}$ as represented in Fig. 9a) by considering the dependency of $E_{oed,i}$ on σ'_{33}[28]:

$$\delta\varepsilon_{33} = \sum_i \frac{\delta \log \sigma'_{33}}{(1+e_{0,i})} \cdot C_{c,i} \cdot \vartheta_i \qquad 9$$

where $e_{0,i}$ is the initial void ratio of the i layer.

In addition, the total axial strain, $\delta\varepsilon_{33}$, can be computed from the specimen compressibility index. Therefore equation (9) can be rewritten as:

$$\delta\varepsilon_{33} = \frac{\delta \log \sigma'_{33}}{(1+e_0)} \cdot C_c \qquad 10$$

where e_0 is the void ratio of the entire specimen (equations in the Appendix), and C_c is the specimen compressibility index.

Combining Equation (10) and Equation (9), one can derive the relationship between the compressibility indices of the specimen and those of the layers:

$$C_c = (1+e_0)\sum_i \frac{C_{c,i} \cdot \vartheta_i}{(1+e_{0,i})} \qquad 11$$

4.2. Post-yield behaviour evolution with the composition

To identify the post-yield behaviour of each layer (linear in the semi-logarithmic plane $\log\sigma'_{33}$-e), two parameters are needed: the layer compressibility ($C_{c,i}$) and a reference void ratio ($e_{1,i}$) defined at the vertical effective stress of 1 MPa, prolonging the post-yield compression line, with slope $C_{c,i}$ (Fig. 9a).

These layer parameters were calibrated with the results of shaly and sandy specimens from the Mont Terri URL.[12,15] In Fig. 9b, two experimental oedometric curves are reported: a specimen from the shaly facies of the Mont Terri URL[15] and a specimen from Lausen borehole[12] with a similar clay content (≈61% wt.).

As for the drained elastic parameters, the shaly layer parameters correspond to those of a shaly specimen. The parameters of the sandy layer were back-calculated adopting Equation (11) and the information on the shaly and sandy volumetric fractions, and the results are reported in Table 2.

For each shaly volumetric fraction, the reference void ratio is computed (equation in the appendix), while C_c is calculated with Equation (11).

Fig. 10 compares the modelled and experimental compressibility indices. The compressibility indices of several specimens coming from three investigation sites are reported: the Lausen borehole, 6–70 m depth,[12] the Schlattingen borehole, 830–970 m depth, (SLA) and the Mont Terri Rock Laboratory, 300 m depth (MT).[12,15] In the three sites, the Opalinus Clay is found at different depths, and the formation has been subjected to different loading histories. The interpretation of the material behaviour as a layered structure is consistent with the increase in experimental compressibility with the shaly volumetric fraction. The different loading histories are likely to be among the causes of the disagreement between the model and experiments. The data for specimens from the greater depth (SLA) lies in the lower part of the group of points, and the layered structure model overestimates the compressibility. However, a limited number of points for each site is available, which may hinder a dependence on the diagenetic processes.

It has to be noted that the approach considers a maximum clay mineral content of 67 wt% (material composed of 100% shaly layers). In one case, a specimen with an even higher clay content (approximately

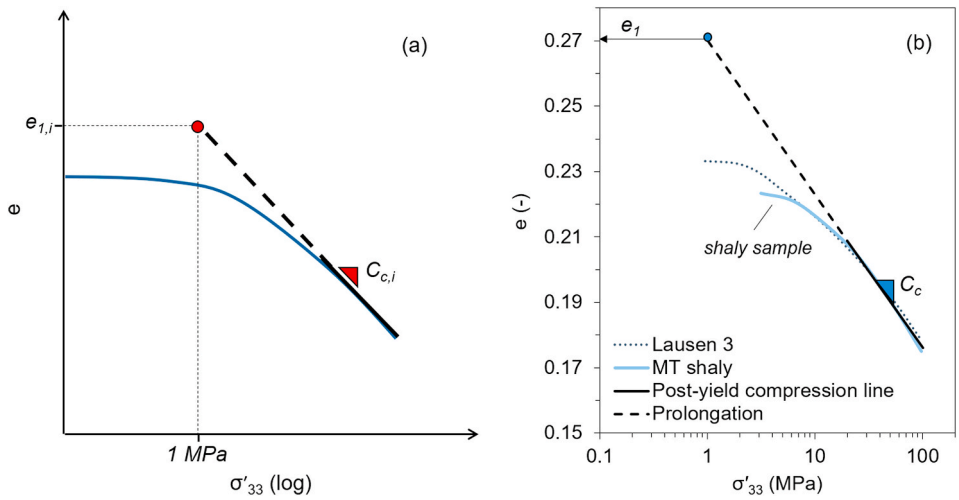

Fig. 9. (a) Compressibility index and reference initial void ratio for the ith layer; (b) example on a shaly specimen (corresponding to the response of a shaly layer). Experimental data from Ref 16 (MT shaly) and 12 (Lausen 3).

Table 2
Reference void ratio and compressibility index for sandy and shaly layers in post-yield conditions.

	Sandy layer	Shaly layer
$e_{1,i}$ (-)	0.13	0.27
$C_{c,i}$ (-)	0.008	0.047

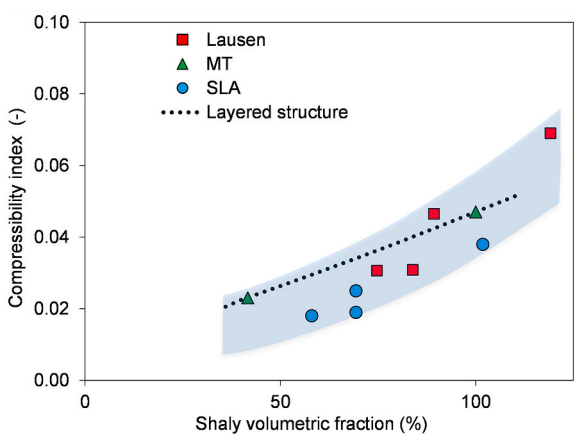

Fig. 10. Comparison between the estimated compressibility index Cc for a layered material and the experimental results. Experimental data from Refs. 12, 15. The shaded region is a visual aid for reading the graph.

80 wt%) was tested. For these specimens, the proposed model would simulate the material as a 120% shaly volumetric fraction, which is above the maximum possible value, while the actual geomaterial may have a different structure compared to the one proposed in Section 2.

5. Shear strength

The strength of Opalinus Clay specimens from Mont Terri, tested in saturated triaxial conditions are herein analysed, and the effect of the mineralogy is investigated, assuming the layered composition presented in Section 2. During shearing at constant strain rate, the deviatoric stress increased until reaching a maximum (peak strength). After the peak, the deviatoric stress decreases until reaching a constant value, hereafter referred to as ultimate (or post-peak) strength.

Empirical correlations are drawn between the shaly volumetric fraction and the peak and ultimate strengths.

5.1. Strength evolution with the composition

The results obtained from drained[11,14] and undrained saturated triaxial tests[35] are summarised in Fig. 11. All results refer to specimens coming from the Mont Terri URL (approximately 300 m in depth), which were loaded in the direction perpendicular to the bedding planes. For some tests, either the peak or the ultimate shear strength was not available (e.g. in multistage tests). Therefore, not all points in the peak strength plot have a corresponding value in the ultimate strength plot and vice versa.

The clouds of points show an apparent dispersion of the results, which can be primarily explained when grouping the points by specimen composition. The results in the plot are categorised based on the shaly volumetric fraction. The specimens with a similar composition (shaly volumetric fraction within ±3%) have been grouped, and the results have been linearly interpolated adopting Mohr Coulomb failure criterion. The effective cohesion, c', and the mobilized shear strength, ϕ', evolution with the shaly volumetric fraction is shown in Fig. 12.

For a lower shaly volumetric fraction, as the coarser mineral components increase, the ϕ' increases (Fig. 12a). A power law interpolation for ϕ' (°) was obtained from the available data. For the parameter c', data were not sufficient to determine a dependency on the composition and is therefore assumed constant. Parameters for the interpolation at peak and ultimate strength are reported in Table 3.

For the peak strength, ϕ' ranges from 44° for the low shaly volumetric fraction to 24° for the 100% shaly specimens, and c' is 2.2 MPa. For the ultimate shear strength, ϕ' ranges from 35° to 17° and $c' = 1$ MPa.

The shape of the ϕ' and c' functions for the ultimate shear strength are similar to the ones found for the peak shear strength, although shifted towards lower values. A relevant change in the strength occurs in the intercept parameter (here, c'), which is reduced by more than 50% compared to the peak condition. This reduction can be attributed to the loss of cementation in the specimens after the peak, which reduces the shear strength significantly. The validity of the parameters derived for the failure criteria refers to the analysed stress range and is based on the available data. A larger amount of data for the low shaly volumetric fraction would allow the empirical correlation parameters to be refined, particularly in the mean effective stress range lower than 10 MPa.

Using the power law interpolation of the ϕ' parameter, the peak and ultimate shear strengths can be determined as surfaces in a 3D space: the deviatoric stress, mean effective stress and shaly volumetric fraction. As

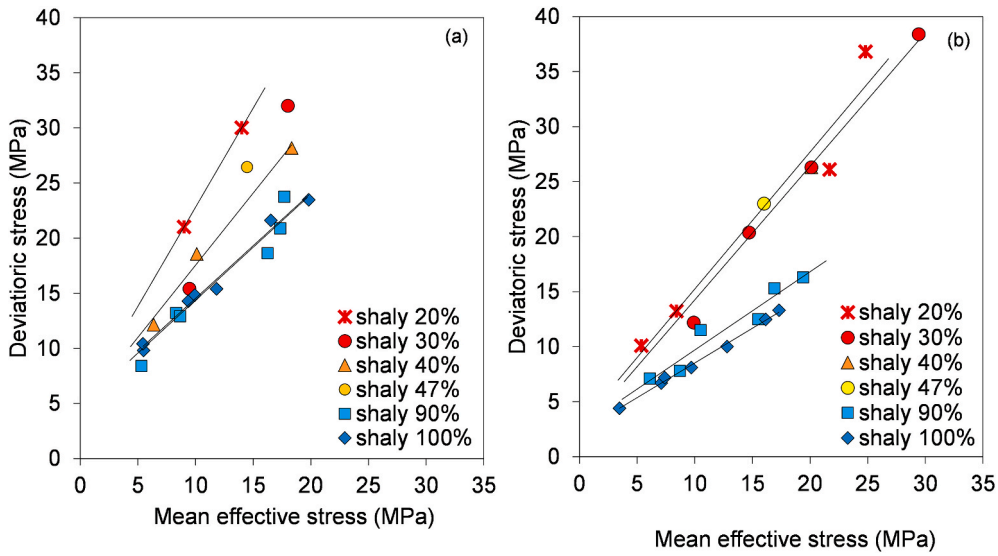

Fig. 11. Peak (a) and ultimate (b) shear strengths for all the analysed tests, grouped by the shaly volumetric fraction.

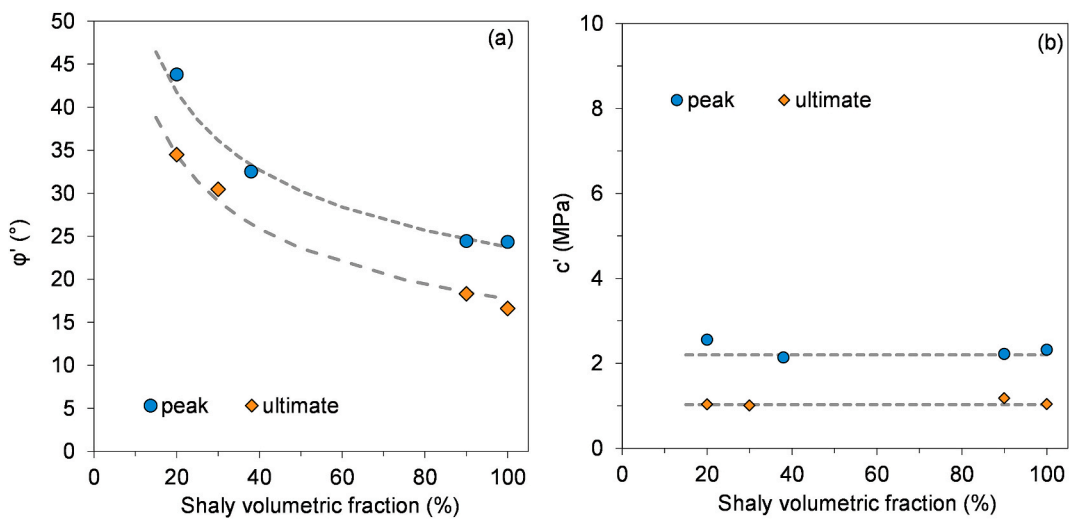

Fig. 12. Evolution of the parameters (a) ϕ′ and (b) c′ with the shaly volumetric fraction for the regression lines at the peak and ultimate conditions.

Table 3
Strength parameters at the peak and ultimate conditions; a power law is used to express the empirical correlation between the shaly volumetric fraction and the parameter ϕ′ (°).

	$\phi' = x \cdot \vartheta_{shaly}^{-y}$		c′ (MPa)
	x (-)	y (-)	
Peak	120	0.35	2.2
Ultimate	119	0.41	1.0

an example, the surface for the peak shear strength is shown in Fig. 13a. The corresponding contour lines are shown in the *q*-*p*′ plane in Fig. 13b. The coloured curves are labelled with the corresponding shaly volumetric fraction. The lower the shaly volumetric fraction is, the higher the peak (and ultimate) shear strength is, because of the increasing friction angle.

The accuracy of the developed correlations is hereafter evaluated. The calculated peak and ultimate shear strengths are plotted versus the measured values in Fig. 14 (a, b). The results from undrained and drained tests are reported. The interpolating surfaces led to a good approximation of the shear strength in the peak and ultimate conditions. The interpolation is particularly suitable for the peak shear strength, where the error is limited to ±10%.

Based on the available data, it, therefore, appears possible to estimate the shear strength of the formation (peak and ultimate) with the only input of the clay-mineral content (i.e., shaly volumetric fraction) of the specimen.

6. Conclusion

In this work, the literature information on the structure and composition of Opalinus Clay specimens are interpreted, and a layered structure of the shale is proposed. The shale is defined as characterised by shaly-type and sandy-type layers with a given composition, porosity and hydromechanical parameters. Based on this structure, the information on the mineralogical composition is used to determine the shaly volumetric fraction, i.e., the amount of shaly-type layer in the overall specimen.

Experimental results in triaxial and oedometric conditions are analysed to determine the dependence of the mechanical parameters on the shaly volumetric fraction. The higher the shaly fraction is, the lower the

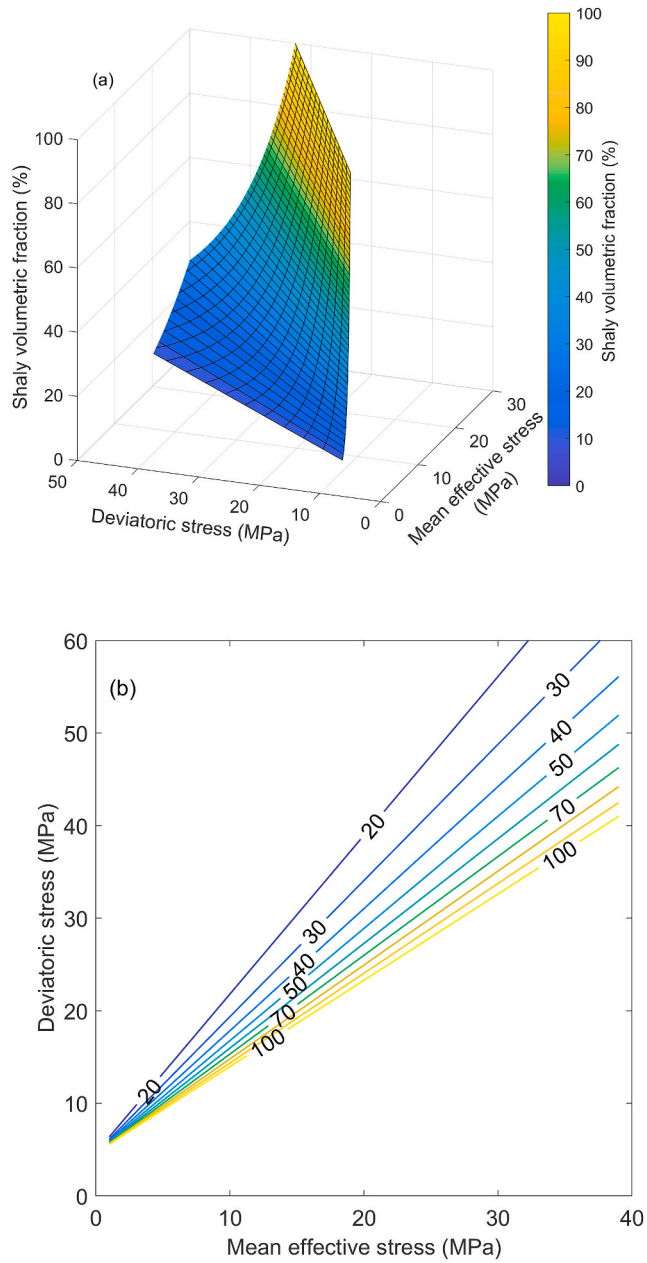

Fig. 13. (a) Peak strength in the three-dimensional space: deviatoric stress, mean effective stress, and shaly volumetric fraction. Colour highlights the shaly volumetric fraction to help in reading the graph. (b) Peak strength in mean effective versus deviatoric stress plane, contour plots of the 3D surface in panel (a). Labels on the lines refer to the shaly volumetric fraction (%). (For interpretation of the references to colour in this figure legend, the reader is referred to the Web version of this article.)

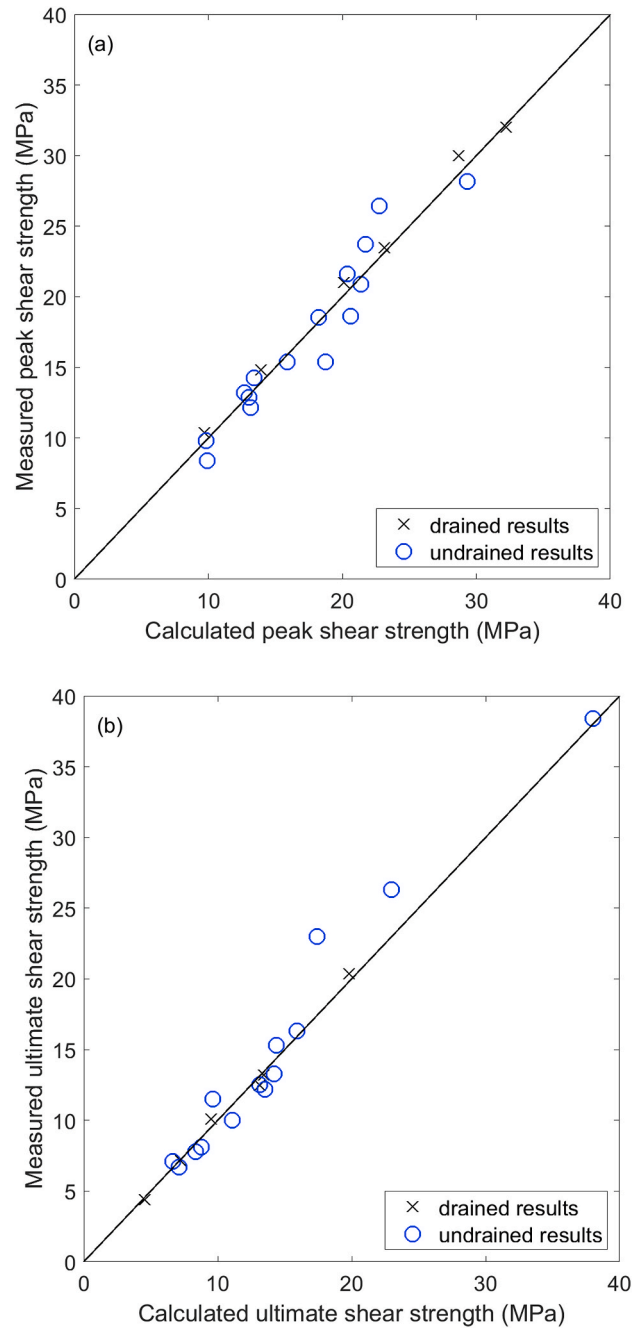

Fig. 14. Comparison between the measured and computed shear strengths at (a) peak and (b) ultimate conditions. The blue circles refer to the undrained results; the black crosses refer to the drained results (i.e., Refs. 11,14). (For interpretation of the references to colour in this figure legend, the reader is referred to the Web version of this article.)

stiffness, the lower the peak and ultimate shear strengths and the higher the shale compressibility.

The elastic properties of the transversely isotropic material are determined by adopting an analytical solution for materials with a layered structure. The stress dependency of the elastic parameters is considered, and the values are calibrated on results obtained in triaxial drained conditions. The undrained elastic parameters are computed and compared to experimental results. Good correspondence is found when adopting Skempton's B coefficient of 0.8, which is compatible with the experimental finding in the analysed stress range. This approach allows evaluating, with a low computational cost, the nonlinear elastic properties of a transversely isotropic layered material, considering a wide range of compositions and confining stresses of interest for the practical application.

The elastoplastic compressibility of Opalinus Clay specimens in the oedometric condition is interpreted as a layered structure by attributing compressibility and porosity values to each layer type. The combination of layers is analytically solved and compared to the experimental results. The correlation well adapts to the more superficial specimens, while for the ones sourced from a greater depth, the correlation tends to overestimate the compressibility.

The peak and ultimate strengths of many tests performed in drained or undrained shearing conditions, on specimens coming from the same

site, are subdivided into homogenous groups based on the shaly volumetric fraction. For each group, the parameters for the Mohr-Coulomb failure criterion are determined and related to the shaly volumetric fraction via empirical correlations. The correlation allows estimating the shear strength of the formation with the only input of the clay-mineral content (i.e., shaly volumetric fraction) of the specimen.

The approach shows that the properties of Opalinus Clay can be predicted with good approximation adopting a layered structured approach at the centimetre scale. In conclusion, most of the variability in the experimental results for the hydromechanical parameters of Opalinus Clay can be justified by the specimen composition.

This approach can be used to estimate the properties of the specimens before testing and therefore to guide the choice of the experimental tests to perform. Moreover, it may be extended, as is, by combining the analytical and empirical correlations to information on the shale composition at a larger scale, maintaining the advantage of a low computational cost. Estimates of the specimen compositions are nowadays also available on the decimetre to metre scale via calibrated tomography scans[26] and the database on log data is currently growing. By combining this approach with log data, the presented approach can potentially be extended to a larger scale to obtain a map of the hydromechanical properties of the shale at the investigation site scale, allowing for the evaluation of the parameters to be assigned in large scale modelling approaches, as for the application to the tunnel excavation for radioactive waste disposal.

Declaration of competing interest

The authors declare that they have no known competing financial interests or personal relationships that could have appeared to influence the work reported in this paper.

Acknowledgements

The support of the Swiss National Cooperative for the Disposal of Radioactive Waste (NAGRA) for this research is acknowledged. The authors wish to acknowledge the laboratories participating in the benchmark study for having provided the data used in this work: SINTEF Formation Physics laboratory, NGI laboratory, Gesteinslabor Dr. Eberhard Jahns, ETH Zurich Institute of Geotechnics, and the RSTD Co.

Appendix. Shaly and sandy volumetric fraction derivation

In the following, the relationships between the phases (Fig. A1) and the derivation of the shaly and sandy volumetric fractions, i.e., the volume percentages of the shaly and sandy layers in a specimen, are shown.

The derivation moves from the definition of the mineralogical mass contents of clay and non-clay (the complement of the clay mineral amount to the total amount), which are the results usually obtained from a mineralogical analysis (e.g., from X-ray diffractometry). This input is converted to the shaly and sandy volumetric fractions, assuming a fixed mineralogical composition and porosity, for each layer kind.

The clay mineral x_c and non-clay mineral x_{nc} contents by mass are defined as follows:

$$x_c = M_{s,c} / M_s \tag{12}$$

$$x_{nc} = M_{s,nc} / M_s \tag{13}$$

where $M_{s,c}$ and $M_{s,nc}$ are the solid mass of the clay and non-clay minerals, respectively, and M_s is the total solid mass.

The solid density ρ_s is computed as follows:

$$\frac{1}{\rho_s} = \frac{x_c}{\rho_{s,c}} + \frac{x_{nc}}{\rho_{s,nc}} \tag{14}$$

where $\rho_{s,c}$ and $\rho_{s,nc}$ are the average clay mineral and average non-clay mineral densities, respectively.

The above-defined densities allow the content by weight to be converted to the solid volume fraction (i.e., porosity excluded) of the clay ($\widetilde{\phi}_c$) and non-clay ($\widetilde{\phi}_{nc}$) components:

$$\widetilde{\phi}_c = V_{s,c} / V_s = x_c \cdot \rho_s / \rho_{s,c} \tag{15}$$

$$\widetilde{\phi}_{nc} = V_{s,nc} / V_s = x_{nc} \cdot \rho_s / \rho_{s,nc} \tag{16}$$

where $V_{s,c}$ is the clay mineral volume, $V_{s,nc}$ is the non-clay mineral volume, and V_s, is the total solid volume.

For each layer type, the solid volume ($V_{s,shaly}$ or $V_{s,sandy}$) is given by the sum of the solid volume of clay $V_{s,c}$ and non-clay minerals $V_{s,nc}$:

$$V_{s,shaly} = V_{s,c,shaly} + V_{s,nc,shaly} \tag{17}$$

$$V_{s,sandy} = V_{s,c,sandy} + V_{s,nc,sandy} \tag{18}$$

The parameters a and b are defined as the volumetric fractions of clay content attributed to the shaly and the sandy layers, respectively:

$$a = V_{s,c,shaly} / V_{s,shaly} \tag{19}$$

$$b = V_{s,c,sandy} / V_{s,sandy} \tag{20}$$

The void ratios of the shaly and sandy layers are defined as follows:

$$e_{shaly} = V_{v,shaly} / V_{s,shaly} \tag{21}$$

$$e_{sandy} = V_{v,sandy} / V_{s,sandy} \tag{22}$$

Where the subscript v indicates the voids (i.e., the volume of voids in the shaly and sandy layers). The void ratio of the entire specimen is defined as follows:

$$e = V_V / V_s \tag{23}$$

Starting from the mineralogical and microstructural analysis reported in Ref. 23; the reference compositions and void ratios for the shaly and sandy layers were adopted:

- shaly layer: $a = 65\%$, void ratio $e_{shaly} = 0.23$
- sandy layer: $b = 15\%$, void ratio $e_{sandy} = 0.11$.

The solid volume fractions of clay $\widetilde{\phi}_c$ and non-clay minerals $\widetilde{\phi}_{nc}$ are obtained from the solid volume fractions of shaly $\widetilde{\phi}_{shaly}$ and sandy layers $\widetilde{\phi}_{sandy}$, assuming the average composition and porosity of each kind of layer. The fractions are obtained as follows:

$$\begin{aligned} \widetilde{\phi}_c &= a \cdot \widetilde{\phi}_{shaly} + b \cdot \widetilde{\phi}_{sandy} \\ \widetilde{\phi}_{nc} &= (1-a) \cdot \widetilde{\phi}_{shaly} + (1-b) \cdot \widetilde{\phi}_{sandy} \end{aligned} \tag{24}$$

where $\widetilde{\phi}_{shaly}$ and $\widetilde{\phi}_{sandy}$ are

$$\begin{aligned} \widetilde{\phi}_{shaly} &= \left(V_{s,c,shaly} + V_{s,nc,shaly}\right) \Big/ V_s \\ \widetilde{\phi}_{sandy} &= \left(V_{s,c,sandy} + V_{s,nc,sandy}\right) \Big/ V_s \end{aligned} \tag{25}$$

Equation (23) can be rewritten as $e = e_{shaly} \cdot \widetilde{\phi}_{shaly} + e_{sandy} \cdot \widetilde{\phi}_{sandy}$, adopting the solid volume fraction definitions.

The shaly and sandy volumetric fractions, i.e., the volume of the shaly layers and sandy layers, respectively, over the total volume (V), can now be defined considering the porosity attributed to each layer type:

$$\vartheta_{shaly} = \frac{V_{s,shaly} + V_{v,shaly}}{V} = \frac{\widetilde{\phi}_{shaly}}{1+e}\left(1 + e_{shaly}\right) \tag{26}$$

$$\vartheta_{sandy} = \frac{V_{s,sandy} + V_{v,sandy}}{V} = \frac{\widetilde{\phi}_{sandy}}{1+e}\left(1 + e_{sandy}\right) \tag{27}$$

The sum of the two fractions is equal to one.

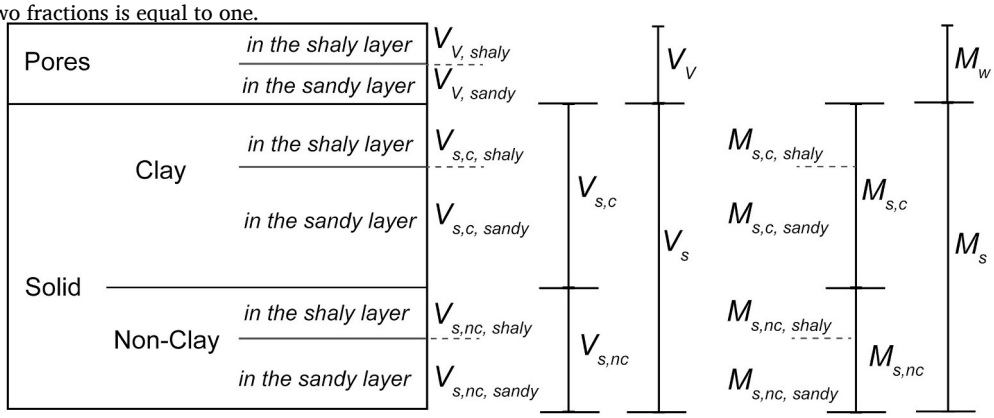

Fig. A1. Relationships among the phases for Opalinus Clay, considering shaly and sandy layers. Saturated condition (volumes, V, and masses, M). The subscript s and v indicate respectively the solid phase and the porous phase. The second subscript c or nc indicates clay and non-clay mineral (total amount minus the clay minerals). The shaly and sandy subscripts refer to the corresponding layers. For example, $V_{s,nc,sandy}$ is the volume of solid, other than clay minerals, within the sandy layer.

References

1 Adhikary DP, Dyskin AV. Modelling of progressive and instantaneous failures of foliated rock slopes. *Rock Mech. Rock Eng. Wien.* 2007;40:349–362. https://doi.org/10.1007/s00603-006-0085-8.

2 Adhikary DP, Dyskin AV. A Cosserat continuum model for layered materials. *Comput Geotech.* 1997;20:15–45.

3 Amadei B, Stephansson O. *Rock Stress and its Measurement.* Springer Netherlands; 1997. https://doi.org/10.1007/978-94-011-5346-1.

4 Barden L. Stresses and displacements in a cross-anisotropic soil. *Geotechnique.* 1963; 13:198–210. https://doi.org/10.1680/geot.1963.13.3.198.

5 Biarez J, Favre JL. *Table ronde sur les corrélations des paramètres en mécanique des sols.* Paris: Ecole Cent; 1972.

6 Bishop AW, Hight DW. The value of Poisson's ratio in saturated soils and rocks stressed under undrained conditions. *Geotechnique.* 1977;27:369–384. https://doi.org/10.1680/geot.1977.27.3.369.

7 Bossart P, Thury M. *Mont Terri Rock Laboratory. Project, Programme 1996 to 2007 and Results.* 2008.

8 Burland JB. On the compressibility and shear strength of natural clays. *Geotechnique.* 1990;40:329–378.

9 Chiu HK, Johnston IW, Donald IB. Appropriate techniques for triaxial testing of saturated soft rock. *Int J Rock Mech Min Sci Geomech Abstr.* 1983;20:107–120. https://doi.org/10.1016/0148-9062(83)91301-3.

10 Chou PC, Carleone J, Hsu CM. Elastic constants of layered media. *J Compos Mater.* 1972;6:80–93.

11 Crisci E. *Hydro-mechanical response of Opalinus Clay shale: dependency on composition and burial dept. h.* 2019. https://doi.org/10.5075/epfl-thesis-7421. EPFL thesis.

12 Crisci E, Ferrari A, Giger SB, Laloui L. Hydro-mechanical behaviour of shallow Opalinus Clay shale. *Eng Geol.* 2019;251:214–227. https://doi.org/10.1016/j.enggeo.2019.01.016.

13 David EC, Brantut N, Schubnel A, Zimmerman RW. Sliding crack model for nonlinearity and hysteresis in the uniaxial stress–strain curve of rock. *Int J Rock Mech Min Sci.* 2012;52:9–17. https://doi.org/10.1016/j.ijrmms.2012.02.001.

14 Favero V, Ferrari A, Laloui L. Anisotropic behaviour of Opalinus clay through consolidated and drained triaxial testing in saturated conditions. *Rock Mech Rock Eng.* 2018;51:1305–1319. https://doi.org/10.1007/s00603-017-1398-5.

15 Ferrari A, Favero V, Laloui L. One-dimensional compression and consolidation of shales. *Int J Rock Mech Min Sci.* 2016;88:286–300. https://doi.org/10.1016/j.ijrmms.2016.07.030.

16 Ferrari A, Favero V, Marschall P, Laloui L. Experimental analysis of the water retention behaviour of shales. *Int J Rock Mech Min Sci*. 2014;72:61–70. https://doi.org/10.1016/j.ijrmms.2014.08.011.

17 Ferrari A, Minardi A, Ewy R, Laloui L. Gas shales testing in controlled partially saturated conditions. *Int J Rock Mech Min Sci*. 2018;107:110–119. https://doi.org/10.1016/j.ijrmms.2018.05.003.

18 Gautschi A. Safety-relevant hydrogeological properties of the claystone barrier of a Swiss radioactive waste repository: an evaluation using multiple lines of evidence. *Grundwasser*. 2017;22:221–233. https://doi.org/10.1007/s00767-017-0364-1.

19 Gerrard CM. Equivalent elastic moduli of a rock mass consisting of orthorhombic layers. *Int J Rock Mech Min Sci Geomech Abstr*. 1982;19:9–14. https://doi.org/10.1016/0148-9062(82)90705-7.

20 Giger SB, Ewy RT, Favero V, Stankovic R, Keller LM. Consolidated-undrained triaxial testing of Opalinus Clay: results and method validation. *Geomech. Energy Environ.* 2018;14:16–28. https://doi.org/10.1016/j.gete.2018.01.003.

21 Gräsle W, Plischke I. *LT-A Experiment: Mechanical Behavior of Opalinus Clay, Data Report from Phase 15 (No. Mont Terri Project, Technical Note 2010-86)*. Germany: BGR; 2011.

22 Gräsle W, Plischke I. *LT Experiment: Mechanical Behavior of Opalinus Clay, Final Report from Phases 6 – 14 (No. Mont Terri Project, Technical Report 2009-07)*. Germany: BGR; 2010.

23 Houben ME, Desbois G, Urai JL. A comparative study of representative 2D microstructures in Shaly and Sandy facies of Opalinus Clay (Mont Terri, Switzerland) inferred form BIB-SEM and MIP methods. *Mar Petrol Geol*. 2014;49:143–161. https://doi.org/10.1016/j.marpetgeo.2013.10.009.

24 Hu DW, Zhang F, Shao JF, Gatmiri B. Influences of mineralogy and water content on the mechanical properties of argillite. *Rock Mech Rock Eng*. 2013;47:157–166. https://doi.org/10.1007/s00603-013-0413-8.

25 Kaufhold A, Gräsle W, Plischke I, Dohrmann R, Siegesmund S. Influence of carbonate content and micro fabrics on the failure strength of the sandy facies of the Opalinus Clay from Mont Terri (Underground Rock Laboratory). *Eng Geol*. 2013;156:111–118. https://doi.org/10.1016/j.enggeo.2013.01.014.

26 Keller LM, Giger SB. Petrophysical properties of Opalinus clay drill cores determined from med-XCT images. *Geotech Geol Eng*. 2019;37:3507–3522. https://doi.org/10.1007/s10706-019-00815-2.

27 Kim KY, Zhuang L, Yang H, Kim H, Min K-B. Strength anisotropy of berea sandstone: results of X-ray computed tomography, compression tests, and discrete modeling. *Rock Mech Rock Eng*. 2016;49:1201–1210. https://doi.org/10.1007/s00603-015-0820-0.

28 Lambe TW, Whitman RV. *Soil Mechanics*. John Wiley & Sons; 1969.

29 Lauper B, Jaeggi D, Deplazes G, Foubert A. Multi-proxy facies analysis of the Opalinus Clay and depositional implications (Mont Terri rock laboratory, Switzerland). *Swiss J Geosci*. 2018;111:383–398. https://doi.org/10.1007/s00015-018-0303-x.

30 Lings ML. Drained and undrained anisotropic elastic stiffness parameters. *Geotechnique*. 2001;51:555–565.

31 Mazurek M, Wersin P, Hadi J. *Opalinus Clay in the Shallow Decompaction Zone: Geochemical Investigations on Drill Core Samples from Borehole Lausen KB (No. NAB 16-58)*. 2017.

32 Menaceur H, Delage P, Tang A-M, Conil N. The thermo-mechanical behaviour of the Callovo-Oxfordian claystone. *Int J Rock Mech Min Sci*. 2015;78:290–303. https://doi.org/10.1016/j.ijrmms.2015.07.002.

33 Minardi A, Crisci E, Ferrari A, Laloui L. Anisotropic volumetric behaviour of Opalinus clay shale upon suction variation. *Géotech Lett*. 2016;6:144–148. https://doi.org/10.1680/jgele.16.00023.

34 Minardi A, Ferrari A, Ewy R, Laloui L. Nonlinear elastic response of partially saturated gas shales in uniaxial compression. *Rock Mech Rock Eng*. 2018;51. https://doi.org/10.1007/s00603-018-1453-x, 1967–1978.

35 Minardi A, Ferrari A, Laloui L. *Benchmark Study on Triaxial Testing of Opalinus Clay: Analysis and Comparative Evaluation of Tests Results. Nagra Arbeitsbericht NAB 19-018*. Wettingen: Nagra; 2019.

36 Minardi A, Giger SB, Ewy RT, et al. Benchmark study of undrained triaxial testing of Opalinus Clay shale: results and implications for robust testing. *Geomech. Energy Environ*. 2020;100210. https://doi.org/10.1016/j.gete.2020.100210.

37 Nagra. Projekt Opalinuston. Synthese der geowissenschaftlichen Untersuchungsergebnisse. *Technischer Bericht*; 2002, 02-03 https://www.nagra.ch/data/documents/database/dokumente/$default/Default%20Folder/Publikationen/NTBs%202001-2010/d_ntb02-03.pdf.

38 Peters M, Mazurek M, Jaeggi D, Müller HR. *WS-H Experiment: Heterogeneities in the Sandy Facies of Opalinus Clay on a Scale of Millimeters to Centimetres (Mont Terri Technical Note No. TN 2010-76)*. University of Bern; 2011.

39 Pham QT, Vales F, Malinsky L, Nguyen Minh D, Gharbi H. Effects of desaturation–resaturation on mudstone. *Phys Chem Earth, Parts A/B/C*. 2007;32:646–655. https://doi.org/10.1016/j.pce.2006.03.012.

40 Philipp T, Amann-Hildenbrand A, Laurich B, Desbois G, Littke R, Urai JL. The effect of microstructural heterogeneity on pore size distribution and permeability in Opalinus Clay (Mont Terri, Switzerland): insights from an integrated study of laboratory fluid flow and pore morphology from BIB-SEM images. *Geol. Soc. Lond. Spec. Publ.* 2017;454:85–106. https://doi.org/10.1144/SP454.3.

41 Pickering DJ. Anisotropic elastic parameters for soil. *Geotechnique*. 1970;20:271–276. https://doi.org/10.1680/geot.1970.20.3.271.

42 Salager S, François B, Nuth M, Laloui L. Constitutive analysis of the mechanical anisotropy of Opalinus Clay. *Acta Geotech*. 2013;8:137–154. https://doi.org/10.1007/s11440-012-0187-2.

43 Salamon MDG. Elastic moduli of a stratified rock mass. *Int J Rock Mech Min Sci Geomech Abstr*. 1968;5:519–527. https://doi.org/10.1016/0148-9062(68)90039-9.

44 Seiphoori A, Whittle AndrewJ, Krakowiak KonradJ, Einstein HerbertH. Insights into diagenesis and pore structure of Opalinus shale through comparative studies of natural and reconstituted materials. *Clay Clay Miner*. 2017;65:135–153. https://doi.org/10.1346/CCMN.2017.064055.

45 Talesnick ML, Katz A, Ringel M. An investigation of the elastic stress-strain behavior of a banded sandstone and a sandstone-like. *Material. Geotech. Test. J.* 2000;23:257–273. https://doi.org/10.1520/GTJ11050J.

46 Wild KM, Wymann LP, Zimmer S, Thoeny R, Amann F. Water retention characteristics and state-dependent mechanical and petro-physical properties of a clay shale. *Rock Mech Rock Eng*. 2015;48:427–439. https://doi.org/10.1007/s00603-014-0565-1.

47 Wittke W. *Felsmechanik*. Springer-Verlag; 1984.

48 Zimmerman RW. The effect of microcracks on the elastic moduli of brittle materials. *J Mater Sci Lett*. 1985;4:1457–1460. https://doi.org/10.1007/BF00721363.

49 Lisjak Andrea, et al. Numerical Modelling of the Anisotropic Mechanical Behaviour of Opalinus Clay at the Laboratory-Scale Using FEM/DEM. *Rock Mechanics and Rock Engineering*. 2014;47:187–206. https://doi.org/10.1007/s00603-012-0354-7.